

# High-resolution migration history of the Subtropical High/Trade Wind system of the northeastern Pacific during the last ~55 years: Implications for glacial atmospheric reorganization

Heather Cheshire<sup>1</sup> and Juergen Thurow<sup>1</sup>

Received 3 September 2012; revised 19 May 2013; accepted 22 May 2013; published 27 June 2013.

[1] Guaymas Basin, Gulf of California, is a restricted basin located under the present-day wet/dry subtropical divide (~27°N) and is ideally circumstanced for detecting variations in the North Pacific Subtropical High (NPSH)/Trade Wind system. Controlled by climate cell boundary displacement, NPSH midwinter location was the primary influence on timing and intensity of upwelling seasons in Guaymas Basin. Analysis of high-resolution X-ray fluorescence data and sediment fabric log from 75% laminated Core MD02-2517/2515, western Guaymas Basin, reveals systematic changes in NPSH behavior over the last ~55 kyr BP. Southward displacement of the wet/dry subtropical divide controlled upwelling-related diatom productivity, while sea level and regional rainfall controlled terrigenous supply. The basin was oxic during the glacial, and preservation was ensured by high burial rate due to the increased deposition of terrigenous sediment. Sediment fabric style (number and/or thickness of laminae, plus color banding and homogeneous intervals) changes systematically through the core and gives insights into the number of seasons occurring in Guaymas Basin, and the occurrence and intensity of the upwelling season. Five millennial-scale low flux events with close timing to Heinrich events and ten decadal/centennial-scale low biogenic silica events occurring in the interval ~33–16.5 kyr BP are interpreted as times of extreme aridity. At ~16.5 kyr BP, a regime shift from terrigenous-dominated oxic to evenly balanced biogenic-terrigenous dysoxic conditions occurred. Although there was a further extreme arid event at ~11.5 kyr BP, ~16.5 kyr BP was essentially the beginning of the interglacial.

**Citation:** Cheshire, H., and J. Thurow (2013), High-resolution migration history of the Subtropical High/Trade Wind system of the northeastern Pacific during the last ~55 years: Implications for glacial atmospheric reorganization, *Paleoceanography*, 28, 319–333, doi:10.1002/palo.20031.

## 1. Introduction

[2] Investigations of the North Pacific's role in the last glaciation have focused on the age of water masses, ventilation, productivity, salinity, and sea surface temperatures. Interestingly, all of the parameters that show significant glacial-interglacial variation are intimately linked with the Subtropical High/Trade Wind system.

[3] Guaymas Basin, Gulf of California (Figure 1), a restricted basin located under the present-day wet/dry subtropical divide (~27°N), is ideally circumstanced for detecting variations in the North Pacific Subtropical High (NPSH)/Trade Wind system. In modern times, the basin experiences a high seasonal contrast due to the NPSH annual migration; it has exceptional sedimentation rates, high

productivity, and high preservation potential along the flanks of the basin where the oxygen minimum zone coincides with low oxygen Pacific Intermediate Water [Thunell *et al.*, 1993; 1995; Pike and Kemp, 1997; Pride *et al.*, 1999; Keigwin, 2002]. Modern sedimentation is intimately linked to the seasonal cycle, and, as a result, annual varves are preserved [Calvert, 1966; Baumgartner *et al.*, 1991; Thunell *et al.*, 1993]. Variations in NPSH behavior have the potential to impact on upwelling (productivity and preservation), rainfall/runoff (terrigenous flux), and seasonality (sediment fabric). Glacial to interglacial shifts of the Intertropical Convergence Zone (ITCZ) in the Pacific have been previously proposed [Leduc *et al.*, 2009; McClymont *et al.*, 2012], which, by implication, include reorganization of the NPSH High/Trade Wind system. In our view, restrictions on the geographical extent of the NPSH/Trade Wind system would have had a marked effect on the number, intensity, and duration of seasons in Guaymas Basin.

[4] In this paper, we report the results of a high-resolution X-ray fluorescence (XRF) scan and a high-resolution sediment fabric log of Core MD02-2515 and ~6 m long kasten Core MD02-2517 from Guaymas Basin (see Figure 1 for core location). We use the data to construct a systematic

Additional supporting information may be found in the online version of this article.

<sup>1</sup>Department of Earth Sciences, University College London, London, UK.

Corresponding author: H. Cheshire, Department of Earth Sciences, University College London, Gower Street, London WC1E 6BT, UK. (h.cheshire@ucl.ac.uk)

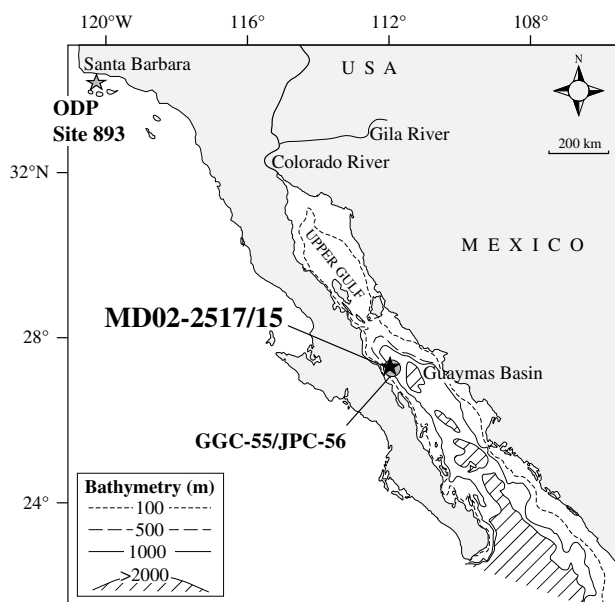


**Figure 1.** Guaymas Basin and location of Site MD02-2517/2515. The 100 m bathymetric contour reveals the shallowness of the Upper Gulf of California and how much further south the Colorado River delta would have been during the glacial.

overview of climatically significant variations in the migration of the NPSH, the evolution of regional climate over the last ~55 kyr BP, and connections with large-scale climate processes.

## 2. Background

[5] Guaymas Basin (~27°N, ~112°W) is the largest of a series of fault-bounded basins within the Gulf of California (Figure 1). Sill depth to the south is ~1500 m, giving open access to low-oxygen Pacific Intermediate Water (~500–1000 m), which is imported due to the regional excess of evaporation over precipitation [Bray, 1988]. Sill depth to the north, bounding the shallow Upper Gulf, is ~500 m. Nutrient-rich waters are flushed into Guaymas Basin by the high tidal range in the Upper Gulf [Lluch-Cota, 2000; Lavin et al., 1998; Kowalewski et al., 2000], and nutrients are seasonally enhanced by NPSH-driven upwelling [Dean et al., 2004].

[6] Midwinter NPSH location is ~23°N [Reid et al., 1958]. In early February, it expands and begins a northward migration, during which its onshore winds drive a moving high-productivity upwelling cell that reaches ~48°N at midsummer. In July, the NPSH contracts and begins a southward migration, during which its onshore winds cause water column overturn [Reid et al., 1958]. To the north of the modern wet/dry subtropical divide, summers are windy with occasional coastal fog, and winters are wet. To the south of the divide, winters are dry with strong winds from late November to late March, while the mostly calm, hot summers are punctuated by occasional evaporation-forced convective storms. Guaymas Basin is slightly to the south of the modern divide. Almost all of its rainfall (<80 mm yr<sup>-1</sup>) occurs in late summer [Thunell et al., 1996], during which, tidal mixing provides nutrients for relatively low-level productivity comprising slow-growing large diatoms and coccolithophores, while high temperatures build water column stratification [Sancetta,

1995]. In November, northwesterly NPSH winds cause thermocline breakdown, and diatom frustules produced over summer are deposited [Thunell, 1998; Dean et al., 2004]. The subsequent nutrient overturn causes a diatom bloom of mixed species [Sancetta, 1995]. The strongest winds over Guaymas Basin are experienced February–March [Pares-Sierra et al., 2003], when upwelling occurs in eastern Guaymas Basin and nutrients are transported in surface waters across to western Guaymas Basin [Hammann et al., 1988]. High productivity resulting from this comprises fast-growing upwelling diatom species [Sancetta, 1995]. Nutrients are recycled in surface waters, and deposition of diatom frustules begins when upwelling ceases in March.

[7] Guaymas Basin sediment trap data [Thunell et al., 1993, 1994; Sancetta, 1995; Thunell, 1998] reveal that organic carbon is suspended in the water column until July–August when it adheres to clay particles [Thunell, 1998] that originate from desert dust lofted during convective storms [Baba et al., 1991] and is deposited. Colorado River sediment is trapped in the Upper Gulf (on average less than 300 m deep; Figure 1) [Lavin et al., 1998; Alvarez et al., 2009], and very little modern terrigenous sediment reaches Guaymas Basin via this route. However, Dean et al. [2004] have shown that during the latest Holocene, northern Guaymas Basin received a small proportion of its terrigenous sediment flux via the Colorado River.

## 3. Materials and Methods

### 3.1. Core MD02-2517/2515

[8] In 2002, ~63 m-long Marion Dufresne continuous piston core, MD02-2515 (27°29.10'N, 112°04.46'W; 888 m water depth; Figure 1), and companion ~6 m long kasten core, MD02-2517 (27°29.01'N, 112°04.64'W; 881 m water depth), were retrieved on the MONA expedition (IMAGES VIII) [Beaufort et al., 2002]. The composite core is ~75% laminated, making it ideal for high-resolution geochemical and sediment fabric analyses.

[9] Overlapping 20 cm images were taken using an overhead fixed camera [Schaaf and Thunell, 1994; Beaufort et al., 2002]. Gas-expansion gaps in Core MD02-2515 were measured using ImageJ software (<http://rsb.info.nih.gov/ij/>) and subtracted from the shipboard depth-scale to establish a void-corrected depth-scale; there are no gaps in Core MD02-2517, the top of which is the sediment-water interface.

### 3.2. Geochemical Analyses

[10] The split core sections were scanned using a CORTEX XRF scanner (at the University of Bremen, 2003). The method integrates the results under the incident X-ray beam (in this study, 1 cm<sup>2</sup>) and produces semiquantitative elemental intensities in counts per second [Jansen et al., 1998; Röhl and Abrams, 2000].

[11] Three samples were taken downcore every 50 cm and were used for quantitative discrete XRF analysis (at the University of Oldenburg) [Tertian and Claisse, 1982], and measurement of biogenic silica and total organic carbon (TOC) content (at the Wolfson Laboratory, University College London). XRF scan data were plotted against discrete XRF data; linear regressions were used to calculate the calibration equations converting the element intensities to concentration data (wt%). Diagenetic and biological

processes have the least affect on Al, a major component of clay minerals and terrigenous flux [Brumsack, 2006]; therefore, element/Al ratios were used to determine sample content relative to standard shale composition [Taylor and McLennan, 1985]. The method used for biogenic silica analysis was Na<sub>2</sub>CO<sub>3</sub> extraction with 2 h heating to dissolve only diatom frustules [USGS Open-File Report 02–371] and molybdate-blue spectrophotometry (absorption peak at 812 nm; precision  $\pm 0.1\%$  at 1 $\sigma$  level) [Shapiro and Brannock, 1962]. For TOC analysis, samples were treated with a 10% solution of hydrochloric acid and combusted in a LECO induction furnace (analytical/internal precision is  $\pm 3.1\%$  at 1 $\sigma$  level).

[12] Geochemical concentration data (wt%) were converted to accumulation rates (g/cm<sup>2</sup>/yr), by multiplying dry bulk density (calculated from wet bulk density data [Beaufort et al., 2002]) and linear sedimentation rate [Gardner et al., 1997].

[13] The modern parameters of biogenic, authigenic, and terrigenous flux in Guaymas Basin are well known from sediment trap and core top data [Thunell et al., 1993, 1994; Sancetta, 1995; Dean, 2006], and fluctuations in their ratios are diagnostic of departures from the modern climate regime (e.g., El Niño–Southern Oscillation (ENSO) events) [Thunell et al., 1996]. In this study, biogenic silica, CaCO<sub>3</sub>, and TOC represent productivity, with the ratio between the first two signifying upwelling or nonupwelling conditions. The authigenic proxies used were MnO/Fe<sub>2</sub>O<sub>3</sub>—Fe oxides readily precipitate in slightly oxic conditions, while Mn oxides only precipitate in significantly oxic conditions [Broecker and Peng, 1982]; vanadium, which precipitates in the same Eh conditions as denitrification [Piper, 1994]; and molybdenum, which, with the assumption that productivity increases bacterial demand for oxygen, coprecipitates with organic matter in dysoxic water columns [Sageman and Lyons, 2003; Dean, 2006]. Terrigenous flux comprises Al<sub>2</sub>O<sub>3</sub>, detrital silica (aluminosilicates and very fine-grained quartz silt; its flux was calculated by subtracting biogenic silica from discrete XRF total silica), and Ti<sub>2</sub>O<sub>3</sub>.

### 3.3. Sediment Fabric Analysis

[14] With the aim of establishing variations in seasonality, a sediment fabric index was developed for core MD02-2517/2515. Its rationale was based on the studies of Holocene varve structure derived from the Back Scattered Electron Imagery (BSEI) study of Core JPC-56 [Pike and Kemp, 1996, 1997, 1999] and the whole core tabulation of the degree of bioturbation of Ocean Drilling Program (ODP) Site 893 [Behl and Kennett, 1996] (Figure 1).

[15] In terms of logging sediment fabrics, simple visual inspection provides too little detail, while scanning electron microscopy (SEM) slide preparation is costly, time consuming, and provides a superfluity of detail. Digital images are a cheap and relatively quick whole-core method; color, contrast, and magnification can be enhanced, and one image comprises a section of core equal to five to six overlapping SEM slides.

[16] Eight sediment fabric types were identified, and every centimeter of the core was assigned to one of the eight categories. Where there were two or more sediment fabric types within 1 cm, it was assigned to the most numerous occurring type. However, there still remain a few centimeter-sections where either the numbers were evenly balanced or the

sediment fabric was transitional between two types. In these instances, the sediment types in the centimeters above and below were taken into consideration. Because experience is the critical factor in obtaining consistent results [Lotter and Lemcke, 1999], logging was repeated three times.

[17] After the age model was established (section 3.5, below), a frequency distribution of sediment fabric types was calculated in order to assess the relative abundance of each type through time. The core was divided into two hundred and twenty 250 year time-slices. Since every centimeter of the core had been assigned to one of the sediment fabric types, the number of “occurrences” of a sediment fabric type in a time-slice could be summed and the dominant type determined.

### 3.4. Accelerator Mass Spectrometry Radiocarbon Analysis

[18] Here we use the 28 Accelerator mass spectrometry (AMS) <sup>14</sup>C dates and age model of Pichevin et al. [2012] produced on 26 marine organic matter samples and two foraminifera samples (Table 1) The analyses were carried out at the Natural Environment Research Council Radiocarbon Facility (Environment), Scottish Universities Environmental Research Centre (SUERC) radiocarbon facility, East Kilbride, Scotland.

[19] Typical precision of SUERC measurements on samples of Holocene age is 30–35 years at 1 $\sigma$ ; samples beyond four half-lives are increasingly less precise due to increasingly smaller amounts of carbon-14 remaining in the sample. MARINE04 software (<http://calib.qub.ac.uk/calib>) [Reimer et al., 2004] was applied to achieve calibration to calendar ages BP for ages prior to 21 kyr, while for older ages, the equation of Bard et al. [2004] was used. Total reservoir ages of 600 years were applied [Berger et al., 1966; Ganeshram et al., 1995].

### 3.5. Age Model

[20] Sedimentation rates for the laminated intervals in Core MD02-2517 were established by measuring varve thicknesses with ImageJ software after the sediment fabric type had been determined. Where possible, three varves per centimeter were measured, and an average thickness for each centimeter was calculated. The number of years per centimeter was calculated by dividing each centimeter by its average varve thickness. Subsequently, sedimentation rate was calculated by dividing each centimeter by the number of years it comprised. Interpolations were made across brief nonlaminated intervals by averaging the rates immediately below and above. This established a “floating” varve chronology for the continuously laminated lower 5 m of core MD02-2517 and the top ~2 m of core MD02-2515.

[21] Upper and lower ages for Core MD02-2515 were established using the AMS radiocarbon dates (Table 1), together with the “floating” chronology for the top 2 m, and linear interpolation between the dated samples.

## 4. Results

### 4.1. Age of Core MD02-2517/2515

[22] Calculation of the number of varves in each centimeter of Core MD02-2517, based on the average varve thickness for each centimeter, yielded ~3000 varve-years for the whole core. The AMS radiocarbon dates for core MD02-2515, varve chronology, and linear interpolation gave an age range

**Table 1.** Radiocarbon  $^{14}\text{C}$  Dates and Calibrated Ages for Core MD02-2515 [Pichevin *et al.*, 2012]

Material	MD02-2515 (m bsf)	MD02-2517/15 (m bsf)	AMS $^{14}\text{C}$ Ages	Error (1 $\sigma$ , years)	Calendar Age (yr BP)
Organic carbon	1.92	13.23	6571	45	6840
Organic carbon	4.26	15.57	7990	37	8256
Organic carbon	6.31	17.62	9438	40	10,077
Organic carbon	8.46	19.77	10,517	42	11,293
Organic carbon	11.19	22.51	12,589	97	13,854
Organic carbon	14.45	25.76	14,767	62	16,894
Organic carbon	20.06	31.38	16,306	164	18,932
Organic carbon	25.20	36.52 <sup>a</sup>	18,397	60	21,007
Foraminifera	25.20	36.52 <sup>a</sup>	18,383	60	20,988
Organic carbon	27.53	38.84	19,471	67	22,391
Organic carbon	29.74	41.06	20,972	78	24,365
Organic carbon	30.71	42.03	22,219	88	25,553
Organic carbon	30.99	42.31	21,994	86	25,303
Foraminifera	36.66	47.97	25,254	121	28,866
Organic carbon	36.66	47.97	25,943	133	29,602
Organic carbon	39.01	50.33	27,425	290	31,165
Organic carbon	43.18	54.51	28,556	335	32,339
Organic carbon	43.46	54.78	29,400	372	33,205
Organic carbon	46.74	58.05	31,519	503	35,669
Organic carbon	47.21	58.52	34,018	662	37,784
Organic carbon	47.93	59.24	35,736	820	39,419
Organic carbon	49.27	60.58	37,484	1023	41,045
Organic carbon	49.82	61.12	38,371	1140	41,855
Organic carbon	50.17	61.49	40,140	1422	43,442
Organic carbon	51.38	62.69	43,584	2184	46,418
Organic carbon	55.06	66.37 <sup>a</sup>	43,940	>3000	49,000
Organic carbon	60.45	71.76	43,940	>3000	52,500
Organic carbon	61.91	73.22	43,905	>3000	54,000

<sup>a</sup>Subhorizontal laminae.

of ~5800–54,600 yr BP. The discrepancy between the ages of the cores indicates a gap of ~2800 years between the top of core MD02-2515 and the bottom of core MD02-2517. Using the average sedimentation rates 50 cm above and below, this represents ~5 m of missing sediment, possibly indicating a recent slump, or that penetration of the sediment began whilst the piston was still blocked at the corer end and hence failed to sample the uppermost layers [Szeréméta *et al.*, 2004]. The age-depth relationship and the sedimentation rate are shown in Figure 2. There are two intervals in the core (~35–38 m and ~66.5–69 m depth) that have subhorizontal laminae. If these represent slumps that brought in extraneous material, this may have implications for the AMS radiocarbon samples taken at these depths.

#### 4.2. Geochemistry

[23] Figure 3 presents the geochemical results as weight percentages (wt%) and accumulation rates together with a summary of the physical appearance of core MD02-2517/2515.

[24] Between ~55 and ~46 kyr BP rates of accumulation across all components were moderate relative to the rest of the core with the exception of a peak of biogenic silica at ~46.5 kyr BP (Figure 3). Highs of calcareous accumulation coincide with lows of biosiliceous accumulation and oxic conditions (notably at ~51 and ~47.5 kyr BP). Accumulation rates of all components fell to their lowest of the whole core between ~46 and ~33 kyr BP. The percentage data show that biogenic components formed the bulk of the sediment ~45–40 kyr BP and terrigenous components predominated ~40–33 kyr BP. From ~38.5 to 35.5 kyr BP, there was low total flux and a trend toward dysoxic conditions. From ~32.5 to 31 kyr BP, there was

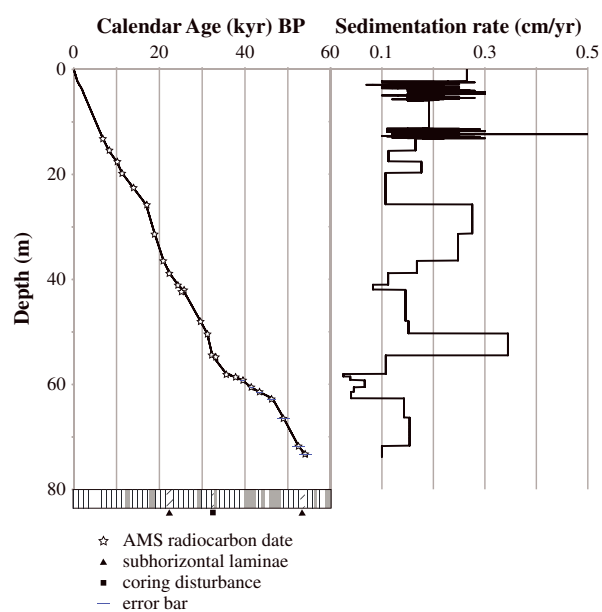


**Figure 2.** Age-depth relationship and sedimentation rate for Core MD02-2517/2515. For data and error bars of AMS radiocarbon dates, see Table S1 in supporting information. Sedimentation rate for Core MD02-2517 and the top 2 m of Core MD02-2515 was calculated from varve thicknesses; sedimentation rate for the rest of Core MD02-2515 was calculated from linear interpolation between AMS radiocarbon dates. AMS radiocarbon dates from Pichevin *et al.* [2012]. Below: a simplified representation of sediment type within the core, including possible slumps and coring disturbance.

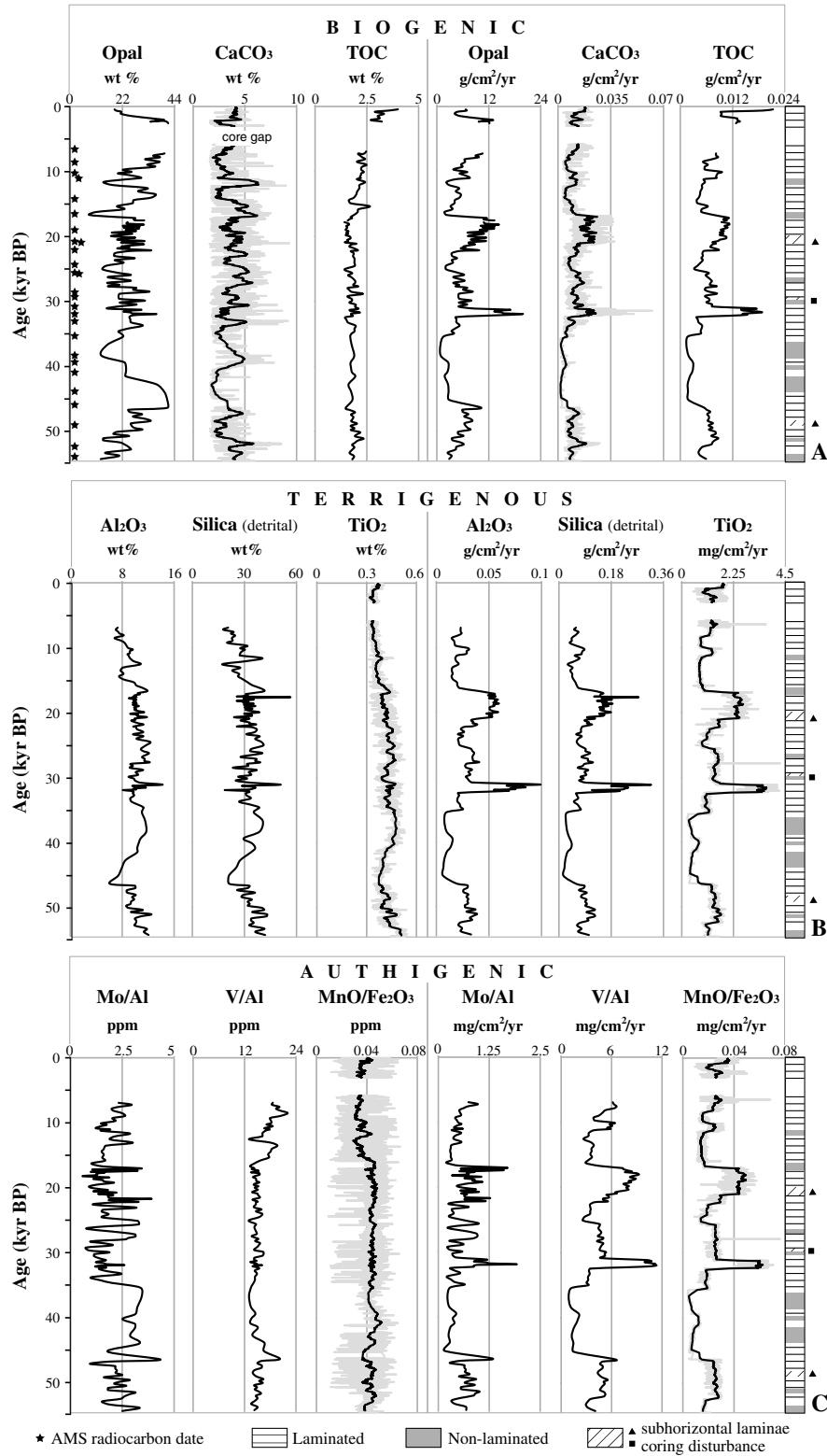


**Figure 3.** (a) (left) Biogenic concentration data (%). (right) Biogenic accumulation rates (g/cm<sup>2</sup>/yr). See Table 2 for statistical analysis. Biogenic silica and TOC are 50 cm-resolution LECO data; CaCO<sub>3</sub> is 1 cm-resolution XRF scanner data. (b) (left) Terrigenous concentration data (%). (right) Terrigenous accumulation rates (Al<sub>2</sub>O<sub>3</sub> and detrital SiO<sub>2</sub>, g/cm<sup>2</sup>/yr; TiO<sub>2</sub>, mg/cm<sup>2</sup>/yr). See Table S2 in supporting information, for statistical analysis. Al<sub>2</sub>O<sub>3</sub> and Detrital SiO<sub>2</sub> are 50 cm-resolution discrete XRF data; TiO<sub>2</sub> is 1 cm-resolution XRF scanner data. (c) (left) Authigenic concentration data (ppm). (right) Authigenic accumulation rates (mg/cm<sup>2</sup>/yr). See Table S2 in supporting information, for statistical analysis. Mo/Al and V/Al are 50 cm-resolution discrete XRF data; MnO/Fe<sub>2</sub>O<sub>3</sub> is 1 cm-resolution XRF scanner data. To the right of each panel is a simplified representation of sediment type within the core.

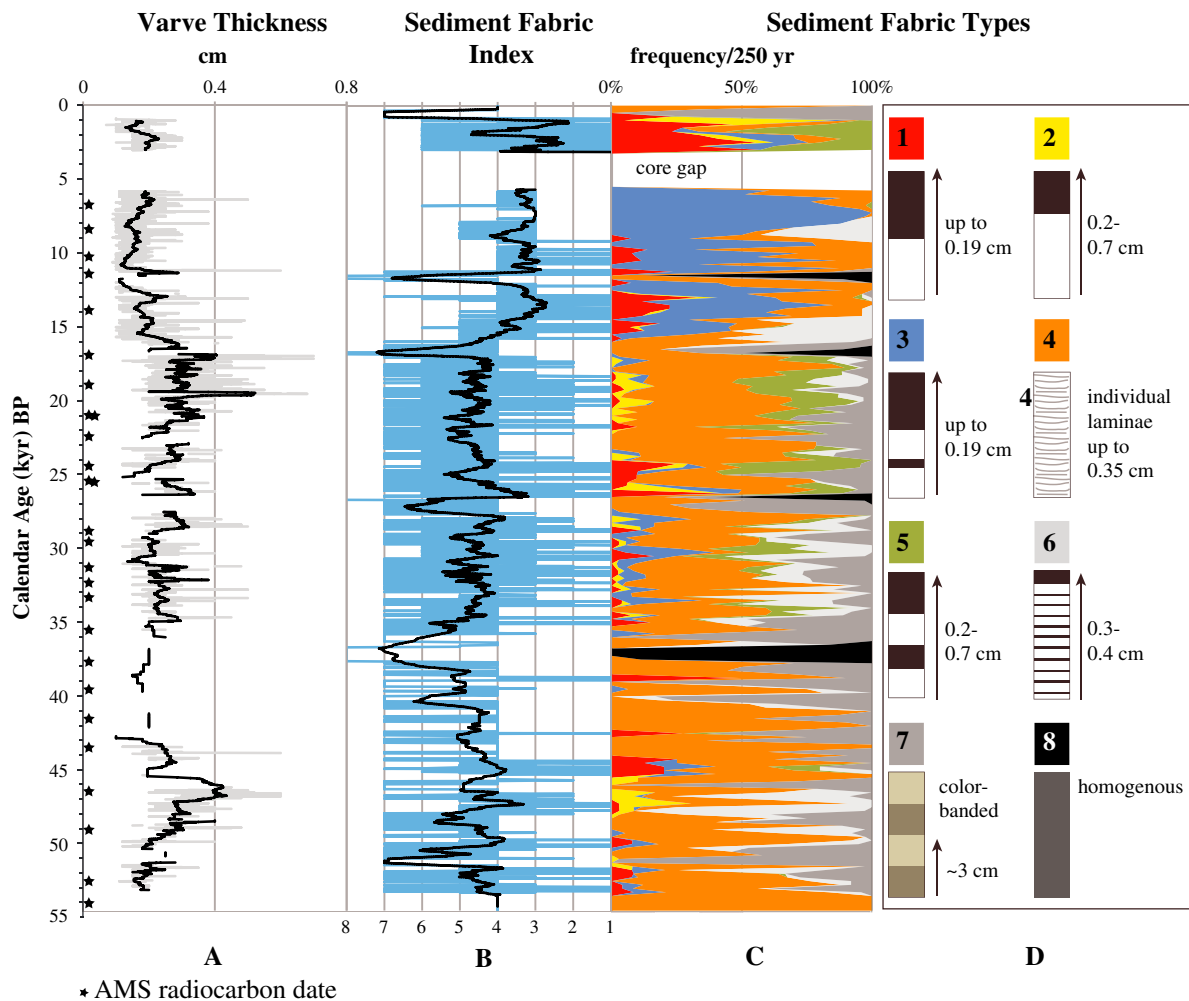


**Figure 4.** Varve thicknesses and sediment fabrics. (a) Varve thicknesses—average per cm. (b) Classification of sediment fabric type for each cm with 25-point running average. (c) Frequency distribution of sediment fabric types in 250 year time-slices. (d) Key to colors and brief description of sediment fabric types.

an interval of very high accumulation rates across all components. There were abrupt millennial-scale events at ~31 kyr BP comprising low biogenic silica and  $\text{CaCO}_3$ , with high terrigenous flux and a trend toward dysoxia and at ~25 kyr BP with low total flux with a trend toward dysoxia. There were decadal/centennial-scale events at ~26, ~20, and ~18.5 kyr BP comprising low biogenic silica and terrigenous flux with high calcareous flux, and decadal/centennial-scale events at ~27, ~21, ~19.3, and 17.9 kyr BP comprising low biogenic silica flux with high terrigenous and calcareous flux. Beginning at ~17 kyr BP, all components fell abruptly and by ~16.5 kyr BP were at their second lowest flux rates of the entire core. Centered on ~16.5 kyr BP, there was a millennial-scale event comprising low total flux with strongly oxic conditions. A millennial-scale event centered on ~11.5 kyr BP was characterized by low biogenic silica accumulation and high terrigenous and  $\text{CaCO}_3$  accumulation with oxic conditions. Although the accumulation rates of all components were relatively low from this point to the top of the core, the percentage data reveal that biogenic silica was the dominant feature.

[25] Broader glacial to interglacial trends show that from ~54.6 to ~16.5 kyr BP, the ratio of average concentration of biogenic to terrigenous components was close to

2:3; from ~16.5 to 0 kyr BP, the ratio was close to 1:1 (Table S1 in supporting information). After ~16.5 kyr BP, the average accumulation of all terrigenous components fell, and, while biogenic silica accumulated at the same rate, TOC accumulation rose and  $\text{CaCO}_3$  accumulation fell. The average concentration of authigenic proxies,  $\text{MnO}/\text{Fe}_2\text{O}_3$  and  $\text{Mo}/\text{Al}$ , was virtually unchanged from glacial to interglacial, whilst that of  $\text{V}/\text{Al}$  rose after ~16.5 kyr BP. The average accumulation rates show that  $\text{MnO}/\text{Fe}_2\text{O}_3$  was unchanged glacial-to-interglacial, while the rates of  $\text{Mo}/\text{Al}$  and  $\text{V}/\text{Al}$  fell slightly.

#### 4.3. Sediment Fabric

[26] The sediment fabric of Core MD02-2517/2515 has three basic states: laminated and color banded; color banded without lamination; and homogeneous (Figure 4). There is large variation within laminated sections, with frequent switching between varved sediment types, all of which may be affected by microbioturbation. A color-banded couplet (light/dark olive-green) is typically 2.5–3 cm thick in the laminated intervals and 4–5 cm thick in the unlaminated color-banded intervals. There are rare instances of burrows.

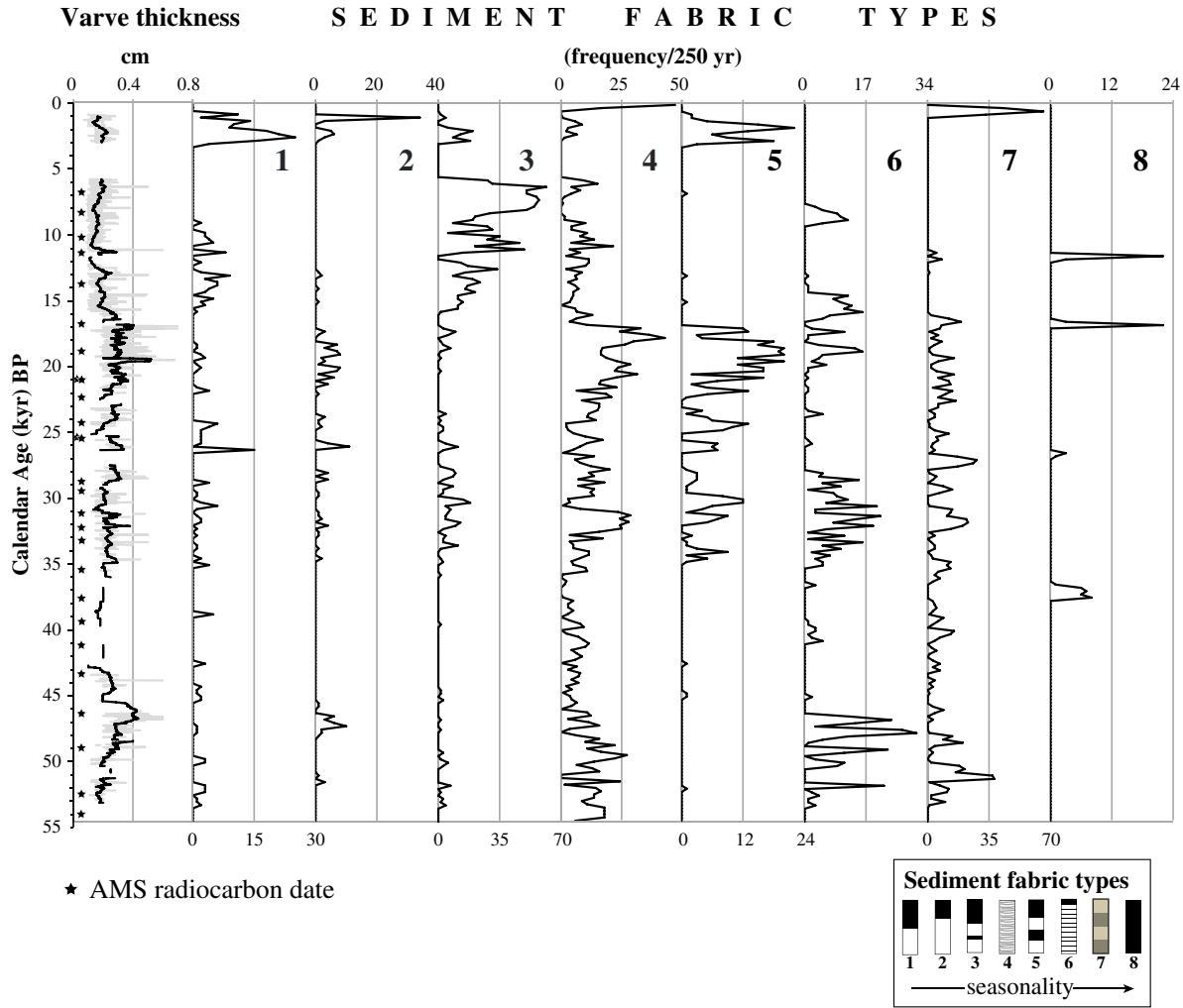


**Figure 5.** The individual sediment fabric types (frequency distribution/250 years) with varve thicknesses for comparison.

[27] The ordering of the sediment fabric types reflects the degree of seasonality: low numbers for high seasonality, high numbers for low seasonality. Sediment fabric **Type 1** (up to ~0.19 cm thick) comprises two laminae of equal thickness. **Type 2** (~0.2–0.7 cm thick) consists of two laminae, with the light one thicker than the dark one. **Type 3** (up to ~0.19 cm thick) comprises four laminae, three of equal thickness (one dark silt rich and two light diatom rich) separated by a thinner silt-rich lamina. **Type 4** consists of alternating light and dark laminae that are too diffuse to assign to any of the laminated sediment types. The assumption was made that poor preservation, rather than low seasonal contrast, was the cause of the diffuse appearance. This may not be the case for all laminae assigned to Type 4; however, there are occasional patches of discontinuous or wavy laminae, and the thicker laminae included in this category probably correspond to low seasonality. **Type 5** (~0.2–0.7 cm thick) comprises four laminae, three of equal thickness (one dark silt rich and two light diatom rich) separated by a thinner silt-rich lamina; type 5 laminae are ~20% thicker than those of the similar type 3. **Type 6** (~0.2–0.7 cm thick) is a quasi two-lamina varve: a relatively thin dark lamina and a very thick lighter

colored lamina containing many very thin silt sublaminæ. **Type 7** is color banded but not laminated. **Type 8** is homogeneous and occurs only four times throughout the entire core. The circumstances of its occurrence at ~27–26.5 kyr BP are ambiguous, and this interval may in fact be an artefact of the coring process.

[28] Figure 5 shows the frequency<sup>-250year</sup> distribution for each sediment fabric type. There is a clear tendency for combinations of sediment types to characterize different intervals. Types 4, 6, and 7 were the most common fabrics ~54–47 kyr BP; types 4, 5, and 6, with minor amounts of 7, characterize ~35–29 kyr BP; between ~24 and 17 kyr BP, types 4 and 5 dominated, with minor amounts of 6 and 7; from ~15 to 6 kyr BP type 3 was the major fabric, with minor amounts of 4 and 1; during the late Holocene, ~3–2.5 kyr BP types 1 and 5 were most common with minor occurrences of 2 and 3. The Latest Holocene was typified by type 7 to ~1 kyr BP. Above this, the sediment is waterlogged and was arbitrarily assigned to type 4 on the assumption that the fabric would be laminated when sufficiently compressed.

[29] During the events at ~51 and ~47.5 kyr BP identified in the geochemical results, the sediment types were 7 and 6, respectively. Across the low flux oxic interval ~38.5–35.5 kyr BP,



the sediment fabric was type 8. Sediment fabric 6 with minor amounts of 4 and 7 occurred during the high flux interval ~32.5–31 kyr BP. Types 4 and 7 dominated the millennial-scale oxic event centered on 29.5 kyr BP, while type 5 characterized the dysoxic event at ~25 kyr BP. The decadal/centennial events at ~29 were typified by sediment fabric type 6, while those at ~26, ~20, and ~18.5 kyr BP were typified by types 4, 5, and 6. Type 7 occurred during the decadal/centennial event at ~27 kyr BP, those at ~21, and ~19.3 kyr BP occurred with types 4 and 5, and the one at ~17.9 kyr BP was dominated by type 4. The millennial-scale low flux oxic event centered on ~16.5 kyr BP was characterized by types 8 and 7, while the low biogenic silica/high terrigenous and high CaCO<sub>3</sub> oxic event centered on 11.5 kyr BP was dominated by type 8 with minor amounts of type 7.

## 5. Discussion

### 5.1. Interpretation of the Sediment Fabric Types

[30] The structure of modern varves—a mm-scale light/dark lamina couplet of equal thicknesses—was revealed by an SEM BSEI study of ~300 mid-Holocene varves from nearby Core JPC-56 (Figure 1) [Pike and Kemp, 1996; 1997; 1999]. The light half-couplet consists of two to three diatom-dominated laminae, reflecting the productivity of different species during spring upwelling, summer stratification, and autumn overturn. The dark half-couplet is silt and organic carbon rich.

[31] Although dysoxic bottom waters resulting from high productivity and the inhibition of bioturbation are widely regarded as prerequisites for the preservation of laminated sediment, investigation of Core GGC-55/JPC-56 (Figure 1) showed that during the Late Glacial, preservation of laminae was not wholly dependent on either productivity or dysoxia. There were times when a high productivity signal was not accompanied by dysoxic conditions; conversely, dysoxia occurred with low preservation of biogenic proxies [Dean, 2006]. Pike and Kemp [1999] suggest that the deposition of “diatom mats” composed of colonial species is a mechanism for varve preservation because their closely packed texture prevents bioturbation.

[32] Despite the subtleties revealed by the ultra-high resolution BSEI study, overall, the modern varve reflects deposition during a high-contrast, two-season annual cycle. Varves with more than two laminae, such as sediment fabric types 3 and 5, are taken to represent an annual cycle with more than two seasons, which is consistent with an equatorward shift of the Hadley climate cell boundary and the imposition of temperate climate over Guaymas Basin. The second silt-rich lamina in sediment fabric types 3 and 5 is an expression of the southward displacement of the NPSH. In modern times, NPSH proximity during winter maintains the wet/dry subtropical divide at ~27°N, but a more southerly location would delay the onset of the upwelling season. Sediment trap data from Santa Barbara Basin [Thunell et al., 1995], located north of the modern wet/dry subtropical divide, show that the upwelling season there in occurs in late spring-summer and that during the fall-winter period there is high lithogenic and low biogenic flux. For the most part, Santa Barbara Basin sediment was not laminated during the last glacial [Hendy and Kennett, 1999] supporting the

hypothesis that the NPSH did not migrate to that latitude. We hypothesize that during the glacial, the NPSH approached Guaymas Basin in late spring-early summer, initiating upwelling; moved past, bringing a spell of low productivity; and then productivity was briefly reinitiated by overturn as it returned on its southward migration to its winter location.

[33] The occurrence of color banding throughout the core suggests that it is an expression of the background Pacific climate. Assuming an average of 10 yr/cm, its ~30 year cyclicity is similar to that of the modern high-pressure/low-pressure Pacific Decadal Oscillation (PDO) [Mantua et al., 1997; Mantua and Hare, 2002; Chavez et al., 2003]. Dean et al. [2004] found cyclicity at PDO scales in terrigenous sediment in Guaymas Basin. The occurrence of type 7 (color banding without lamination) clearly represents times of no distinct annual seasons.

[34] Low-seasonality sediment fabric type 6 represents times when summer was the upwelling season: at the present-day poleward end of the NPSH migration range (Cape Flattery, WA) [Reid, 1958], midsummer upwelling is relatively weak and interrupted by rainy spells. Preservation in this on-off upwelling season could be due to a combination of the deposition of relatively impervious diatom mats and high sedimentation rate [Pike and Kemp, 1999].

[35] The thin-varved types 1 and 3 reflect times equivalent to the modern annual cycle, which is produced by an energetic NPSH that migrates swiftly past Guaymas Basin. The thick-varved types 2, 5, and 6 (and occasionally type 4), by analogy, represent times when a less energetic NPSH passed by more slowly.

### 5.2. Guaymas Basin Climate During the Last ~55 kyr BP

[36] The event at ~47.5 kyr BP (see Figure 6 for details) indicates a period when upwelling either did not occur or was so weak in intensity that diatoms became the subordinate producers. In modern Guaymas Basin, coccolithophore productivity is less than that of diatom species except during ENSO events [Ziveri and Thunell, 2000]. More specifically, upwelling diatom species decrease, and slow-growing tropical species increase while overall productivity decreases [Sancetta, 1995]; annual rainfall and terrigenous flux also increase [Stapp et al., 1999; Thunell, 1998]. Persistent ENSO-like conditions during the glacial have also been reported from the eastern Equatorial Pacific [Koutavas et al., 2002]. It is likely that the conditions there and in Guaymas Basin resulted from the southward displacement of the NPSH/Trade Wind system and the ITCZ due to expansion of the Polar climate cell. Given the margin of error on the adjacent C-14 date, the event at ~47.5 kyr BP is almost coincident with Heinrich event H5. Pichevin et al. [2012], through analysis of  $\delta^{30}\text{Si}$  in a high-resolution record from Core MD02-2515, interpreted this event as an interval of decreased upwelling intensity.

[37] Conditions between ~46 and ~33 kyr BP suggest aridity. During the earlier part of the interval, low levels of productivity indicate that water column overturn delivered nutrients to surface waters, while in the latter part, low accumulation of all components implies intense aridity and water column stratification. Pichevin et al. [2012] record a low in biogenic silica at ~38.5 kyr BP, which



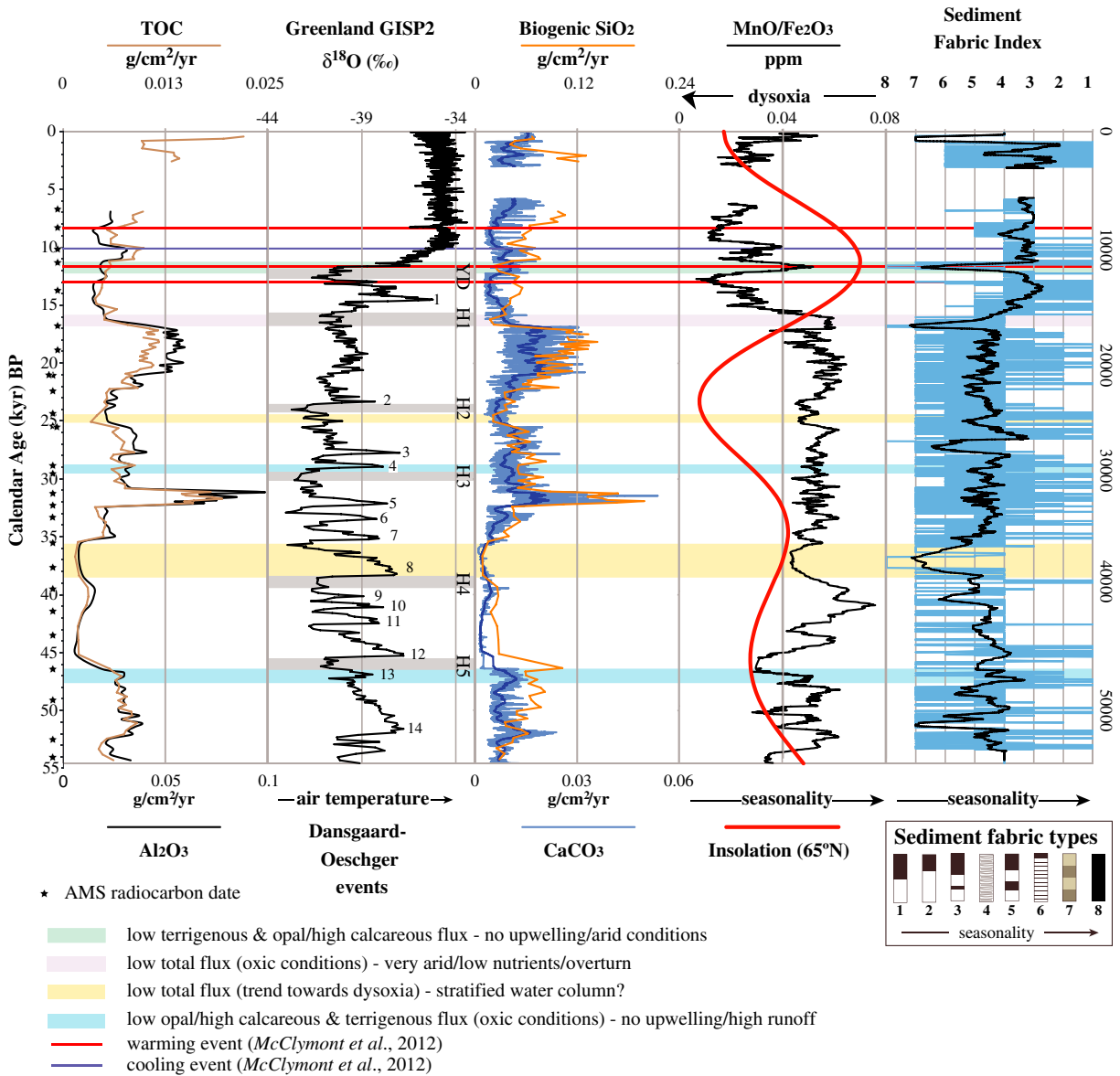


**Figure 6.** Biogenic silica, representing upwelling conditions, and CaCO<sub>3</sub>, representing nonupwelling conditions, compared to terrigenous and TOC flux, Mn/Fe<sub>2</sub>O<sub>3</sub> flux, the sediment fabric index, Northern Hemisphere insolation [Laskar et al., 2004], the GISP2 ice core record [Grootes and Stuiver, 1997], Dansgaard-Oeschger events [Dansgaard et al., 1993], and the Guaymas Basin millennial-scale climatic events [Pichevin et al., 2012; McClymont et al., 2012]. Gray bars are the Younger Dryas event and Heinrich events H1-5.

they equate to Heinrich event H4 (Fig. 6), and interpret as interval of decreased upwelling intensity. During the broader, less well-defined event in our record at ~38–36 kyr BP, the absence of lamination and color banding suggest that the NPSH was not migrating as far as Guaymas Basin.

[38] The North American ice sheets began to readvance at ~33 kyr BP [Kleman et al., 2010]. Ice sheet growth implies falling sea levels, and the Colorado River, cutting down into the Upper Gulf, would have transported remobilized nutrients and terrigenous sediment into Guaymas Basin, boosting productivity and preservation. The millennial-scale events at ~29.5 and ~25 kyr BP (Figure 7) are nearly coincident with Heinrich events H3 and H2. It is possible that the use of linear

interpolation between radiocarbon-dated tiepoints has oversimplified and distorted the age model. Guaymas Basin experienced very low seasonality with high runoff during the first of these events, while aridity and low seasonality were characteristic of the second.

[39] The low biogenic silica flux in the nine decadal/centennial events between ~29 and 17.9 kyr BP (Figure 7) suggests a failure of NPSH migration and seasonal upwelling with concomitant rise in calcareous productivity due to the lack of competition for nutrients. Low terrigenous flux in four of the events suggests aridity; events of this nature only occur during this interval. The ten brief events indicate restriction of the NPSH/Trade Wind system to lower latitudes

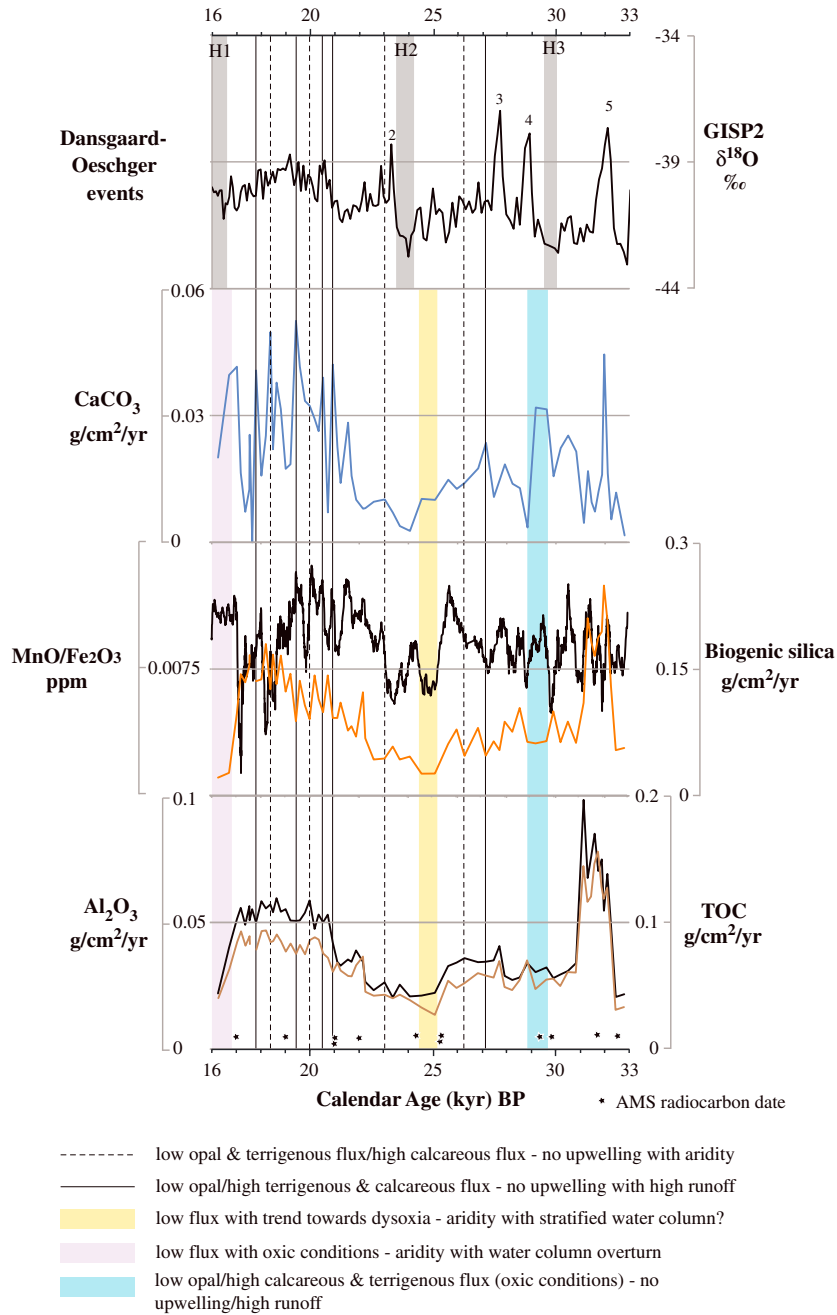


**Figure 7.** ~33–16 kyr BP—biogenic silica, representing upwelling conditions, and  $\text{CaCO}_3$ , representing nonupwelling conditions, compared to terrigenous and TOC flux, the GISP2 ice core record [Grootes and Stuiver, 1997], Dansgaard-Oeschger events [Dansgaard et al., 1993], and the Guaymas Basin millennial-scale climatic events [Pichevin et al., 2012; McClymont et al., 2012]. Gray bars are Heinrich events H1-3. Also shown are 10 decadal/centennial-scale climatic events. Five have low biogenic silica and terrigenous flux with high  $\text{CaCO}_3$  flux (dashed line) and occur exclusively in this interval of Core MD02-2517/2515. Five have low biogenic silica flux with high terrigenous and  $\text{CaCO}_3$  flux.

combined with high runoff rates in the Gulf of California. Two of the millennial-scale low biogenic silica events identified by Pichevin et al. [2012] (~47.5 and ~31 kyr BP) also feature this sediment component ratio.

[40] Most Northern Hemisphere ice sheets attained maximum extent at ~30 kyr BP [Clark et al., 2009]. Although ice retreat began at ~19 kyr BP, the ice sheets on the northwestern continental margins of the Pacific and Atlantic

continued to grow and attained maximum volume at ~16.5 kyr BP [Dyke et al., 2002; Clark et al., 2009; Lambeck et al., 2010]. The sediment fabric types from ~17 to 16 kyr BP suggest that, although upwelling occurred, its intensity was not high and that Guaymas Basin was close to the northward end of NPSH migration range (cf present-day Cape Flattery, WA). The interval ~17.5–16 kyr BP has been defined as the “Big Dry” at Lake Estancia in New Mexico

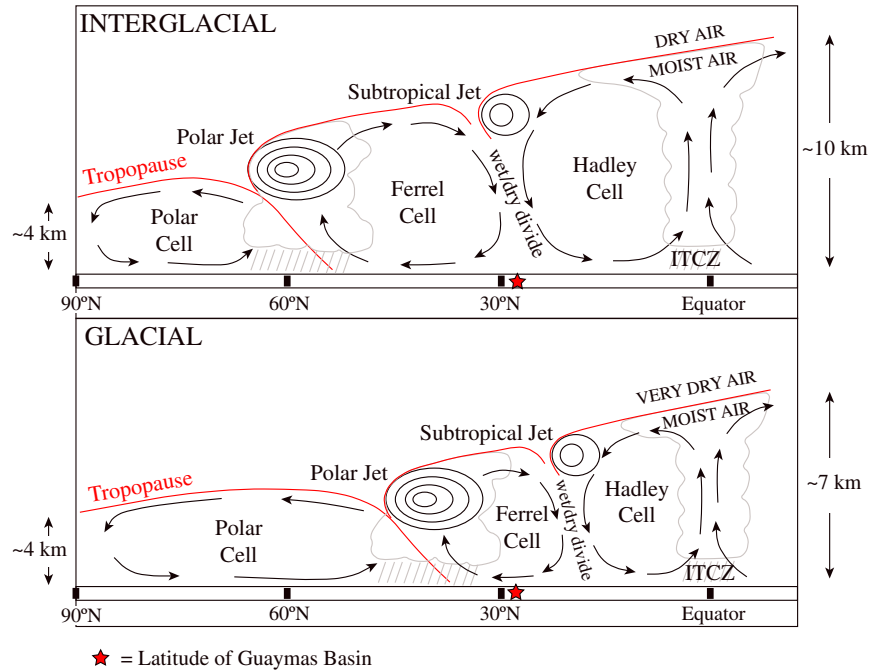


**Figure 8.** The climate cell boundaries. (top) Interglacial climate with the wet/dry subtropical divide centered over ~27°N. (bottom) A possible glacial scenario—frigid climate over the ice sheets dehydrated the atmosphere; the climate cell boundaries and ITCZ were forced equatorward. Consequently, the Trade Winds operated over a smaller area, and less water vapor was lofted at the ITCZ, contributing to atmospheric dehydration. Red star = latitude of Guaymas Basin.

where it is followed by the “Big Wet,” ~16–14.5 kyr BP, together making up the “Mystery Interval,” which has been identified at several other sites [Broecker *et al.*, 2009; Broecker and Putnam, 2012]. The Great Basin Lakes record high water levels through the whole interval with the highest levels attained in the second half [Broecker and Putnam, 2012; Lyle *et al.*, 2012]. There is evidence for aridity and low productivity ~17–16 kyr BP in Guaymas Basin, but not for an exceptional wet episode ~16–14.5 kyr BP. The dry events at Guaymas Basin and Lake Estancia coincide with Heinrich event 1 (H1, Figure 6). Lyle *et al.* [2012] interpret the whole interval in Lake Estancia and the Great Basin Lakes, ~17–14 kyr BP, as increased summer precipitation from moist air masses originating from the tropical Pacific; if this is the case the moisture somehow bypassed the Gulf of California for the interval ~17–16 kyr BP.

[41] After ~15.5 kyr BP, the sediment fabric types indicate that the wet/dry subtropical divide was most probably somewhat to the south of Guaymas Basin and upwelling season was late spring-summer (cf present-day Santa Barbara Basin, CA). Globally, during the Bølling-Allerød interstadial, climate ameliorated and the ice sheets retreated. Northern Hemisphere insolation rose toward its peak at ~11.5 kyr BP. The contraction of the Polar climate cell allowed the boundaries of the tropical and temperate cells to migrate poleward.

[42] The conditions in Guaymas Basin during the Younger Dryas interval suggest that upwelling and diatom productivity collapsed whilst coccolithophore productivity flourished in the absence of competition. The lack of seasonality strongly suggests the failure of the NPSH to migrate as far as Guaymas Basin. Studies of nearby Core

GGC/JPC-56 (Figure 1) corroborate these findings and further suggest that surface water from the Pacific flowed into the Gulf of California. Diatom assemblage showed a radical reduction of upwelling species [Sancetta, 1995] and an increase of open-ocean tropical species [Barron *et al.*, 2005]; terrigenous, organic and CaCO<sub>3</sub> fluxes were high, while biogenic silica flux was low [Barron *et al.*, 2004; Dean, 2006]; and the sediment was not laminated [Keigwin and Jones, 1990; Keigwin, 2002; Barron *et al.*, 2004; 2005; Dean, 2006].

[43] McClymont *et al.* [2012], using temperature proxy U<sub>37</sub><sup>K</sup> and TEX<sub>86</sub><sup>H</sup> analyses on Core MD02-2515, have shown rapid stepped temperature increases during the Late Glacial-Early Holocene in Guaymas Basin with significant rises at ~13, 11.5, and 8.2 kyr BP (Figures 6 and 7). They link these rises to northward shifts of the ITCZ. These intervals show no common characteristics in our geochemical record; the sediment fabric types suggest that the NPSH was energetically migrating to and beyond Guaymas Basin. The interval at ~8.2 kyr BP in our record shows a dysoxic event with high terrigenous accumulation.

[44] Further afield, diachronous south-to-north climate amelioration after ~15 kyr BP reveals the climate cell boundaries slowly migrating northward along the Northeast Pacific Margin. An increase in biogenic flux began off southern California at ~11 kyr BP, while the equivalent increase at ~38°N began at ~7 kyr BP [Gardner *et al.*, 1997]. Glacial coastal air temperatures at ~42°N were ~5°C below present, and they remained low until ~7 kyr BP, while at ~35°N, where glacial air temperatures >10°C lower than present had occurred, air temperatures had risen to near-Holocene values by ~14 kyr BP [Heusser, 1998]. Dysoxia in silled

marginal basins,  $\sim 31\text{--}32^\circ\text{N}$ , reached Holocene levels before the end of MIS 2, while to the north ( $\sim 32\text{--}33^\circ\text{N}$ ) silled basins, experienced enhanced ventilation until  $\sim 4.5$  kyr BP [Stott *et al.*, 2000]; Santa Barbara Basin, a strongly restricted basin at  $34^\circ\text{N}$ , was dysoxic by  $\sim 14$  kyr [Behl and Kennett, 1996]. Denitrification commenced several thousand years earlier at  $\sim 23^\circ\text{N}$  than at  $\sim 42^\circ\text{N}$  [Kienast *et al.*, 2002].

[45] The mid- to Late Holocene in Guaymas Basin saw the establishment of the modern two-season annual cycle, reflected in the prevalence of high seasonality sediment fabric types 1 and 2, and the even ratio of biogenic to terrigenous components.

### 5.3. Likely Sources of High Terrigenous Flux During the Glacial

[46] One of the most prominent features of the Guaymas Basin sedimentary record is the switch over from a terrigenous-dominated system to an even balance between terrigenous and biogenic components at  $\sim 16.5$  kyr BP (Figure 3; Table S2). The increase of insolation due to Milankovitch cyclicity initiated catastrophic melting of ice sheets already destabilized by atmospheric aridity; the release of water rehydrated the atmosphere, re-energized the Subtropical Highs, and the Hadley cell boundaries began to migrate poleward. There are several possible sources for the increased terrigenous flux during the glacial.

[47] 1. With the southward shift of the ITCZ, the Hadley cell boundary, and the less energetic NPSH, the wet-dry subtropical divide was also shifted southward, which brought wet winters and windy fog-bound summers to the central Gulf of California; hence, terrigenous flux increased via high runoff (Figure 8). The southward shift also had the effect of increasing the number of seasons at Guaymas Basin. Evidence from further afield supports the equatorward displacement of the wet/dry subtropical divide. In the eastern North Pacific during MIS 2 and 3, atmospheric reorganization resulted in southward displacement of the ocean gyres [Sabin and Pisias, 1996]. At  $\sim 42^\circ\text{N}$ , subarctic open-ocean diatom and radiolarian species occupied niches currently exploited by coastal upwelling species, and primary production was halved [Sancetta *et al.*, 1992; Sabin and Pisias, 1996; Ortiz *et al.*, 1997]. Decreased denitrification indicates reduced upwelling and better ventilation  $\sim 42^\circ\text{--}23^\circ\text{N}$  [Kienast *et al.*, 2002]. Sediments beneath the modern California Current ( $\sim 42^\circ\text{--}23^\circ\text{N}$ ) recorded a 40% reduction in annual flow [Doose *et al.*, 1997; Herbert *et al.*, 2001]. Increased upwelling and higher productivity between  $\sim 5^\circ\text{--}3^\circ\text{N}$  and  $88^\circ\text{--}87^\circ\text{W}$  [Pedersen *et al.*, 1991; Loubere, 2002] suggest the southward displacement of the Costa Rica Dome [Romero *et al.*, 2011]. Southward shifts of the gyre appear to have occurred on a precessional timescale [Yamamoto *et al.*, 2007].

[48] 2. The Colorado River's flow and sediment load were swollen by higher rainfall and runoff, and, periodically, with glacial meltwater. Southward shift of the climate cell boundaries imposed modern midlatitude wet-temperate climate on the North American southwest (Figure 8), a large part of which is drained by the Colorado River (Figure 1). At  $\sim 20$  kyr BP, there were  $\sim 100$  pluvial lakes in the Great Basin and Mojave Desert [Tchakerian and Lancaster, 2002]. The larger lakes boosted local evaporation and rainfall rates, which in turn drove a positive regional feedback [Hosteller

*et al.*, 1994] through runoff and riverine discharge [van Devender, 1990a, 1990b; Reheis, 1999; Betancourt *et al.*, 2001; Holmgren *et al.*, 2003; Oviatt *et al.*, 2003]: there was  $\sim 133\%$  rainfall over the Colorado Plateau [Anderson *et al.*, 2000] and  $\sim 200\%$  over the Chihuahua and Sonora deserts [Lozano-Garcia *et al.*, 2002; Rhode, 2002; Metcalfe *et al.*, 2002; Menking *et al.*, 2004]. Although Baba *et al.* [1991] have shown that during the latest Holocene, the principal transport agent of Guaymas Basin terrigenous flux was eolian, during the glacial cooler, moister climate over the Sonora Desert promoted montane treecover [Lozano-Garcia *et al.*, 2002; Rhode, 2002; Roy *et al.*, 2012] and desert greening. It is likely that this resulted in lower-than-present eolian transport into Guaymas Basin. Dean *et al.* [2004] have shown that during the latest Holocene, northern Guaymas Basin received at least a portion of its terrigenous sediment flux via the Colorado River. In the Upper Gulf, slow spreading rates over the last  $\sim 5$  Myr [Lonsdale, 1989] have resulted in a gentle bathymetric gradient [Lavin *et al.*, 1998; Alvarez *et al.*, 2009]: a  $\sim 100$  m sea level drop effectively halves its area (Figure 1), shifting the Colorado delta southward with the likelihood of significantly increasing terrigenous deposition in Guaymas Basin.

[49] 3. An additional source of increased accumulation could be that, when sea level was actively lowering, downcutting brought in additional flux via sediment flushing from the Upper Gulf.

## 6. Conclusions

[50] Due to its location close to the wet/dry subtropical divide and the combination of circumstances that create and preserve its annually laminated sediments, Guaymas Basin gives a very rare, possibly unique, opportunity to examine on a millimeter-scale glacial to interglacial climate change—in particular, the behavior of the NPSH at the northern boundary of the Hadley cell. From a human perspective, interglacial climate is the norm, but on an orbital timescale, glacial climate is the norm, and the Guaymas Basin sedimentary record shows a clear distinction between the two.

[51] During the glacial and up to the beginning of the Late Glacial ( $\sim 16.5$  kyr BP), the sediment was dominated by terrigenous flux, and despite high biogenic accumulation (mainly biosiliceous productivity), the basin was oxic; sediment fabrics were predominantly low seasonality laminated and nonlaminated types (mainly Type 7), with minor amounts of high seasonality laminated types.

[52] During the Late Glacial and interglacial, the sediment was evenly balanced between terrigenous and biogenic flux (mainly biosiliceous productivity), and the basin was dysoxic; high seasonality laminated types (mainly Types 1, 2, and 4), with a minor component of nonlaminated types dominated the sediment fabric.

[53] The geochemical record further characterizes the low biogenic silica flux events identified by Pichevin *et al.* [2012]. Conditions were not identical during these events, arguing against a common origin and in favor of those events that do not exactly coincide with Heinrich events actually being local to Guaymas Basin, rather than being mismatched due to inconsistencies in the age model.

[54] The sediment fabric record further characterizes Late Glacial-Early Holocene stepped warming events identified

by *McClymont et al.* [2012]. High seasonality types were laid down during these events indicating that the NPSH/Trade Wind system was fully operational at the latitude of Core MD02-2517/2515.

[55] The most striking thing about the MD02-2517/2515 Guaymas Basin record is the rapid change at ~16.5 kyr BP. At this point, the ratio of terrigenous to biogenic components changed from 3:2 in the glacial to an even balance during the Late Glacial and the Holocene. It is also the point at which varve preservation improves. If it can be assumed that sediment type 4 represents low seasonality, it is also the point at which distinction between the seasons increases and the number of seasons occurring in Guaymas Basin begins to decrease, that is, the wet/dry subtropical divide was established at its modern location. The prevalence of thin varved sediment types indicates an energetic NPSH that moved rapidly past Guaymas Basin and the seasons were brief, but quite distinct.

[56] The insights that the Guaymas Basin record gives into shifts of the Hadley cell boundary are particularly relevant at present. Climate modelling has been used to investigate what could happen due to poleward expansion of the Hadley cell boundary during global climate warming [*Kang and Lu*, 2012]. During the glacial, the southward shifted ITCZ and the geographical restriction on the NPSH/Trade Wind system meant that the NPSH had further to travel in order to reach Guaymas Basin, which had the effect of increasing the number of seasons and/or decreasing seasonal contrasts. Since our record only covers the latter half of the glacial and the Holocene, we cannot categorically state that the situation at ~16.5 kyr BP was mirrored going into the glacial in MIS 4, but it seems likely that it was.

[57] **Acknowledgments.** Many thanks are due to Yvon Balut and the Scientific and Ship's crew of the RV *Marion Dufresne*, MONA Cruise, 2002; Guy Rothwell and Belinda Alker, BOSCORF, University of Southampton; Ursula Röhl and Frank Lamy, Department of Geosciences, University of Bremen; Walter Hale and Alex Wuelbers at the ODP Core Repository, University of Bremen; and Hans Brumsack, University of Oldenburg, for discrete XRF analysis. HC was supported by a PhD studentship from the Department of Earth Sciences, UCL, for most of this research work. Many thanks are also due to John Barron and two anonymous reviewers for their insightful and very helpful comments on an earlier version of this manuscript.

## References

- Alvarez, L. G., F. Suarez-Vidal, R. Mendoza-Borunda, and M. Gonzalez-Escobar (2009), Bathymetry and active geological structures in the Upper Gulf of California, *Bol. Soc. Geol. Mex.*, *61*, 129–141.
- Anderson, R. S., J. L. Betancourt, J. I. Mead, R. H. Hevly, and D. P. Adam (2000), Middle- and late-Wisconsin paleobotanic and paleoclimatic records from the southern Colorado Plateau, USA, *Palaeogeogr. Palaeoclimatol. Palaeoecol.*, *155*, 31–57.
- Baba, J., C. D. Petersen, and H. J. Schrader (1991), Fine-grained terrigenous sediment supply and dispersal in the Gulf of California during the last century, in *The Gulf and Peninsular Province of the Californias*, edited by J. P. Dauphin and B. R. T. Simoneit, Am. Assoc. of Pet. Geol. Mem., *47*, 569–599.
- Bard, E., F. Rostek, and G. Menot-Combes (2004), Radiocarbon calibration beyond 20,000 C-14 yr BP by means of planktonic foraminifera of the Iberian Margin, *Quat. Res.*, *61*, 204–214, doi:10.1016/j.yqres.2003.11.006.
- Barron, J. A., D. Bukry, and J. L. Bischoff (2004), High resolution paleoceanography of the Guaymas Basin, Gulf of California, during the past 15,000 years, *Mar. Micropaleontol.*, *50*, 185–207.
- Barron, J. A., D. Bukry, and W. E. Dean (2005), Paleoclimatic history of the Guaymas Basin, Gulf of California, during the past 15,000 years based on diatoms, silicoflagellates, and biogenic sediments, *Mar. Micropaleontol.*, *56*, 81–102.
- Baumgartner, T. R., V. Ferreira-Bartrina, and P. Hentz-Moreno (1991), Varve formation in the central Gulf of California: A reconsideration of the origin of the dark laminae from the 20<sup>th</sup> century record, in *The Gulf and Peninsular Province of the Californias*, edited by J. P. Dauphin and B. R. Simoneit, Am. Assoc. Pet. Geol. Mem., *47*, 617–636, Tulsa, Okla.
- Beaufort, L., and the Members of the Scientific Party (2002), Cruise Report, MD 126, MONA IMAGES VIII, 453 pp., Inst. Polaire Français Paul-Emile Victor, Plouzané, France.
- Behl, R. J., and J. P. Kennett (1996), Brief interstadial events in the Santa Barbara basin, NE Pacific, during the past 60 kyr, *Nature*, *379*, 243–246.
- Berger, R., R. E. Taylor, and W. F. Libby (1966), Radiocarbon content of marine shells from the California and Mexican west coast, *Science*, *153*, 864–866, doi:10.1126/science.153.3738.864.
- Betancourt, J. L., K. A. Rylander, M. C. Peñalba, and J. L. McVickar (2001), Late Quaternary vegetation history of Rough Canyon, central New Mexico, USA, *Palaeogeogr. Palaeoclimatol. Palaeoecol.*, *165*, 71–95.
- Bray, N. (1988), Thermohaline circulation in the Gulf of California, *J. Geophys. Res.*, *93*, 4993–5020.
- Broecker, W. S., and T.-H. Peng (1982), *Tracers in the sea*, Lamont-Doherty Geol. Obs., Columbia Univ., Palisades, N. Y.
- Broecker, W. S., and A. E. Putnam (2012), How did the hydrologic cycle respond to the two-phase mystery interval?, *Quat. Sci. Rev.*, *57*, 17–25.
- Broecker, W. S., D. McGee, K. D. Adams, H. Cheng, R. L. Edwards, C. G. Oviatt, and J. Quade (2009), A Great Basin-wide dry episode during the first half of the Mystery Interval?, *Quat. Sci. Rev.*, *28*, 2557–2563.
- Brumsack, H.-J. (2006), The trace metal content of recent organic carbon-rich sediments: Implications for Cretaceous black shale formation, *Palaeogeogr. Palaeoclimatol. Palaeoecol.*, *232*, 344–361.
- Calvert, S. E. (1966), origin of diatom-rich, varved sediments from the Gulf of California, *J. Geol.*, *74*, 546–565.
- Chavez, F. P., J. Ryan, S. E. Lluch-Cota, and M. C. Niquen (2003), From anchovies to sardines and back, multidecadal change in the Pacific Ocean, *Science*, *299*, 217–221.
- Clark, P. U., A. S. Dyke, J. D. Shakun, A. E. Carlson, J. Clark, B. Wohlfarth, J. X. Mitrovica, S. W. Hostetler, and A. M. McCabe (2009), The Last Glacial Maximum, *Science*, *325*, 710–714.
- Dansgaard, W., et al. (1993), Evidence for general instability of past climate from a 250-kyr ice-core record, *Nature*, *364*, 218–220.
- Dean, W. E. (2006), The geochemical record of the last 17,000 years in the Guaymas Basin, Gulf of California, *Chem. Geol.*, *232*, 87–98.
- Dean, W. E., C. Pride, and R. Thunell (2004), Geochemical cycles in sediments deposited on the slopes of the Guaymas and Carmen Basins of the Gulf of California over the last 180 years, *Quat. Sci. Rev.*, *23*, 1817–1833.
- van Devender, T. R. (1990a), Late Quaternary vegetation and climate of the Chihuahuan Desert, United States and Mexico, in *Packrat Middens*, edited by J. L. Betancourt, T. R. van Devender, and P. S. Martin, pp. 104–133, Univ. of Ariz. Press, Tucson.
- van Devender, T. R. (1990b), Late Quaternary vegetation and climate of the Sonoran Desert, United States and Mexico, in *Packrat Middens*, edited by J. L. Betancourt, T. R. van Devender, and P. S. Martin, pp. 134–165, Univ. of Ariz. Press, Tucson.
- Doose, H., F. G. Prahl, and M. W. Lyle (1997), Biomarker temperature estimates for modern and last glacial surface waters of the California Current system between 33° and 42° N, *Paleoceanography*, *12*, 615–622.
- Dyke, A. S., J. T. Andrews, P. U. Clark, J. H. England, G. H. Miller, J. Shaw, and J. J. Veillette (2002), The Laurentide and Innuitian ice sheets during the Last Glacial Maximum, *Quat. Sci. Rev.*, *21*, 9–31.
- Ganeshram, R. S., T. F. Pedersen, S. E. Calvert, and J. W. Murray (1995), Large changes in oceanic nutrient inventories from glacial to interglacial periods, *Nature*, *376*, 755–758, doi:10.1038/376755a0.
- Gardner, J. V., W. E. Dean, and P. Dartnell (1997), Biogenic sedimentation beneath the California Current system for the past 30 kyr and its paleoceanographic significance, *Paleoceanography*, *12*, 207–225.
- Grootes, P. M., and M. Stuiver (1997), Oxygen 16/18 variability in Greenland snow and ice with 10<sup>3</sup> to 10<sup>5</sup>-year time resolution, *J. Geophys. Res.*, *102*, 26,455–26,470.
- Hammann, M. G., T. R. Baumgartner, and A. Badon-Dangon (1988), Coupling of the Pacific sardine (*Sardinops sagax caeruleus*) life cycle with the Gulf of California pelagic environment, *Californian Co-operative Oceanic Fisheries Investigations Report*, *29*, pp. 102–109, La Jolla, Calif.
- Hendy, I. L., and J. P. Kennett (1999), Latest Quaternary North Pacific surface-water responses imply atmosphere-driven climate instability, *Geology*, *27*, 291–294.
- Herbert, T. D., J. D. Schuffert, D. Andreasen, L. Heusser, M. Lyle, A. C. Mix, A. C. Ravelo, L. D. Stott, and J. C. Herguera (2001), Collapse of the California Current during glacial maxima linked to climate change on land, *Science*, *293*, 71–75.
- Heusser, L. (1998), Direct correlation of millennial-scale changes in western North American vegetation and climate with changes in the California Current system over the past ~60 kyr, *Paleoceanography*, *13*, 252–262.

- Holmgren, C. A., M. C. Peñalba, K. A. Rylander, J. L. Betancourt, and A. MacKay (2003), A 16,000 <sup>14</sup>C yr BP packrat midden series from the USA-Mexico Borderlands, *Quat. Res.*, *60*, 319–329.
- Hostetler, S. W., F. Giorgi, G. T. Bates, and P. J. Bartlein (1994), Lake-atmosphere feedbacks associated with paleolakes Bonneville and Lahontan, *Science*, *263*, 665–668.
- Jansen, J. H. F., S. J. Van der Gaast, B. Kotscher, and A. J. Vaars (1998), CORTEX, a shipboard XRF scanner for element analyses in split sediment cores, *Mar. Geol.*, *151*, 143–153.
- Kang, S. M., and J. Lu (2012), Expansion of the Hadley Cell under global warming: Winter versus summer, *J. Clim.*, *25*, 8387–8393.
- Keigwin, L. D. (2002), Late Pleistocene-Holocene paleoceanography and ventilation in the Gulf of California, *J. Oceanogr.*, *58*, 421–432.
- Keigwin, L. D., and G. A. Jones (1990), Deglacial climatic oscillations in the Gulf of California, *Paleoceanography*, *5*, 1009–1023.
- Kienast, S., S. E. Calvert, and T. F. Pedersen (2002), Nitrogen isotope and productivity variations along the northeast Pacific margin over the last 120 kyr, surface and subsurface paleoceanography, *Paleoceanography*, *17*(4), 1005, doi:10.1029/2001PA000650.
- Kleman, J., K. Jansson, H. de Angelis, A. P. Stroeven, C. Hattestrand, G. Alm, and N. Glasser (2010), North American ice sheet build-up during the last glacial cycle 115–21 kyr, *Quat. Sci. Rev.*, *29*, 2036–2051, doi:10.1016/j.quascirev.2010.04.021.
- Koutavas, A., J. Lynch-Steiglitz, T. M. Marchitto, and J. P. Sachs (2002), El Niño-like pattern in ice age tropical Pacific sea surface temperature, *Science*, *297*, 226–230.
- Kowalewski, M., G. E. Avila Serrano, K. W. Flessa, and G. A. Goodfriend (2000), Dead river's former productivity: two trillion shells at the mouth of the Colorado River, *Geology*, *28*, 1059–1062.
- Lambeck, K., A. Purcell, J. Zhao, and N.-O. Svensson (2010), The Scandinavian Ice Sheet, from MIS 4 to the end of the Last Glacial Maximum, *Boreas*, *39*, 410–435.
- Laskar, J., P. Robutel, F. Joutel, M. Gastineau, A. C. Correia, and B. Levrard (2004), A long-term numerical solution for the insolation quantities of the Earth, *Astron. Astrophys.*, *428*, 261–285.
- Lavin, M. F., V. M. Godines, and L. G. Alvarez (1998), Inverse-estuarine features of the Upper Gulf of California, *Estuarine Coastal Shelf Sci.*, *47*, 769–795.
- Leduc, G., L. Vidal, K. Tachikawa, and E. Bard (2009), ITCZ rather than ENSO signature for abrupt climate changes across the tropical Pacific, *Quat. Res.*, *72*, 123–131.
- Lluch-Cota, S.-E. (2000), Coastal upwelling in the eastern Gulf of California, *Oceanol. Acta*, *23*, 731–740.
- Lonsdale, P.F. (1989), Geology and tectonic history of the Gulf of California, in *The Geology of North America*, vol. N, *The Eastern Pacific and Hawaii*, edited by E. L. Winterer, D. M. Hussong, and R. W. Decker, pp. 499–521, Geol. Soc. of Am., Denver, Colo.
- Lotter, A. F., and G. Lemcke (1999), Methods for preparing and counting biochemical varves, *Boreas*, *28*, 243–252.
- Loubere, P. (2002), Remote vs local control of changes in the eastern equatorial Pacific bioproductivity from the Last Glacial Maximum to the present, *Global Planet. Change*, *35*, 113–126.
- Lozano-García, M. S., B. Ortega-Guerrero, and S. Sosa-Najera (2002), Mid-to Late-Wisconsin pollen record of San Felipe Basin, Baja California, *Quat. Res.*, *58*, 84–92.
- Lyle, M., L. Heusser, C. Ravelo, M. Yamamoto, J. Barron, N. S. Diffenbaugh, T. Herbert, and D. Andreasen (2012), Out of the Tropics: The Pacific, Great Basin Lakes, and Late Pleistocene water cycle in the Western United States, *Science*, *337*, 1629–1633.
- Mantua, N. J., and S. R. Hare (2002), The Pacific Decadal Oscillation, *J. Oceanogr.*, *58*, 35–44.
- Mantua, N. J., S. R. Hare, Y. Zhang, J. M. Wallace, and R. C. Francis (1997), A Pacific interdecadal climate oscillation with impacts on salmon production, *Bull. Am. Meteorol. Soc.*, *78*, 1069–1079.
- McClymont, E. L., R. S. Ganeshram, L. E. Pichevin, H. M. Talbot, B. E. van Dongen, R. C. Thunell, A. M. Haywood, J. S. Singarayer, and P. J. Valdes (2012), Sea-surface temperature records of Termination 1 in the Gulf of California: Challenges for seasonal and interannual analogues of tropical Pacific climate change, *Paleoceanography*, *27*, PA2202, doi:10.1029/2011PA002226.
- Menking, K. M., R. Y. Anderson, N. G. Shafike, K. H. Syed, and B. D. Allen (2004), Wetter or colder during the Last Glacial Maximum? Revisiting the pluvial lake question in Southwest America, *Quat. Res.*, *62*, 280–288.
- Metcalfe, S. E., A. Say, S. Black, R. McCulloch, and S. L. O'Hara (2002), Wet conditions during the last glaciation in the Chihuahuan Desert, Alta Babicora Basin, Mexico, *Quat. Res.*, *57*, 91–101.
- Ortiz, J. D., A. Mix, S. Hostetler, and M. Kashgarian (1997), The California Current of the Last Glacial Maximum, reconstruction at 42°N based on multiple proxies, *Paleoceanography*, *12*, 191–205.
- Oviatt, C. G., D. B. Madsen, and D. N. Schmitt (2003), Late Pleistocene and early Holocene rivers and wetlands in the Bonneville Basin of western North America, *Quat. Res.*, *60*, 200–210.
- Pares-Sierra, A., A. Mascarenhas, S. G. Marinone, and R. Castro (2003), Temporal and spatial variation of the surface winds in the Gulf of California, *Geophys. Res. Lett.*, *30*(6), 1312, doi:10.1029/2002GL016716.
- Pedersen, T. F., B. Nielsen, and M. Pickering (1991), Timing of Late Quaternary productivity pulses in the Panama Basin and implications for atmospheric CO<sub>2</sub>, *Paleoceanography*, *6*, 657–677.
- Pichevin, L., R. S. Ganeshram, B. C. Reynolds, F. Prah, T. F. Pedersen, R. Thunell, and E. L. McClymont (2012), Silicic acid biogeochemistry in the Gulf of California: Insights from sedimentary Si isotopes, *Paleoceanography*, *27*, PA2201, doi:10.1029/2011PA002237.
- Pike, J., and A. E. S. Kemp (1996), Records of seasonal flux in Holocene laminated sediments, Gulf of California, in *Palaeoclimatology and Palaeoceanography From Laminated Sediments*, edited by A. E. S. Kemp, Geol. Soc. Spec. Publ., *116*, 157–170.
- Pike, J., and A. E. S. Kemp (1997), Early Holocene decadal-scale ocean variability recorded in Gulf of California laminated sediments, *Paleoceanography*, *12*, 227–238.
- Pike, J., and A. E. S. Kemp (1999), Diatom mats in Gulf of California sediments, implications for the palaeoenvironmental interpretation of laminated sediments and silica burial, *Geology*, *27*, 311–314.
- Piper, D. Z. (1994), Seawater as a source of minor elements in black shales, phosphorites and other sedimentary rocks, *Chem. Geol.*, *114*, 95–114.
- Pride, C., R. Thunell, D. Sigman, L. Keigwin, M. Altabet, and E. Tappa (1999), Nitrogen isotopic variations in the Gulf of California since the last deglaciation, response to global climate change, *Paleoceanography*, *14*, 397–409.
- Reheis, M. (1999), Highest pluvial-lake shorelines and Pleistocene climate of the Western Great Basin, *Quat. Res.*, *52*, 196–205.
- Reid, J. L., G. I. Roden, and J. G. Wyllie (1958), Studies of the California Current system, *Californian Co-operative Oceanic Fisheries Investigations Report*, *6*, pp. 28–56, La Jolla, Calif.
- Reimer, P. J., et al. (2004), IntCal04 Terrestrial radiocarbon age calibration, 0–26 cal kyr BP, *Radiocarbon*, *46*, 1029–1058.
- Rhode, D. (2002), Early Holocene juniper woodland and chaparral taxa in the central Baja California Peninsula, Mexico, *Quat. Res.*, *57*, 102–108.
- Röhl, U., and J. J. Abrams (2000), High resolution down hole and non-destructive core measurements from sites 999 and 1001 in the Caribbean Sea, application to the Late Paleocene Thermal Maximum, *Proc. Ocean Drill. Program Sci. Results*, *165*, 191–203.
- Romero, O. E., G. Leduc, L. Vidal, and G. Fischer (2011), Millennial variability and long-term changes of the diatom production in the eastern equatorial Pacific during the last glacial cycle, *Paleoceanography*, *26*, PA2212, doi:10.1029/2010PA002099.
- Roy, P. D., M. Caballero, S. Lozano, O. Morton, R. Lozano, M. P. Jonathan, J. L. Sanchez, and M. C. Macias (2012), Provenance of sediments deposited at Paleolake San Felipe, western Sonora Desert: Implications to regimes of summer and winter precipitation during the last 50 cal kyr BP, *J. Arid Environ.*, *81*, 47–58.
- Sabin, A. L., and N. G. Piasis (1996), Sea surface temperature changes in the northeastern Pacific ocean during the past 20,000 years and their relationship to climate change in northwestern North America, *Quat. Res.*, *46*, 48–61.
- Sageman, B. B., and T. W. Lyons (2003), Geochemistry of fine-grained sediments and sedimentary rocks, in *Treatise on Geochemistry*, vol. 7, *Sediments, Diagenesis and Sedimentary Rocks*, edited by F. T. Mackenzie, pp. 115–158, Elsevier, Amsterdam.
- Sancetta, C. (1995), Diatoms in the Gulf of California, seasonal flux patterns and the sediment record for the last 15,000 years, *Paleoceanography*, *10*, 67–84.
- Sancetta, C., M. Lyle, L. Heusser, R. Zhan, and J. P. Bradbury (1992), Late-Glacial to Holocene changes in winds, upwelling and seasonal position of the Northern California Current system, *Quat. Res.*, *38*, 359–370.
- Schaaf, M., and J. Thuro (1994), A fast and easy method to derive highest-resolution time-series datasets from drillcores and rock samples, *Sediment. Geol.*, *94*, 1–10.
- Shapiro, L., and W. W. Brannock (1962), Rapid analysis of silicate, carbonate and phosphate rocks, USGS Bulletin 1144-A, 56 pp.
- Stapp, P., G. A. Polis, and F. Sanche Pinero (1999), Stable isotopes reveal strong marine and El Niño effects on island food webs, *Nature*, *401*, 468–469.
- Stott, L. D., M. Neumann, and D. Hammond (2000), Intermediate water ventilation on the northeastern Pacific margin during the late Pleistocene inferred from benthic foraminiferal δ<sup>13</sup>C, *Paleoceanography*, *15*, 161–169.
- Széréméta, N., F. Bassinot, Y. Balut, L. Labeyrie, and M. Pagel (2004), Oversampling of sedimentary series collected by giant piston core, evidence and corrections based on 3.5-kHz chirp profiles, *Paleoceanography*, *19*, PA1005, doi:10.1029/2002PA000795.

CHESHIRE AND THUROW: GLACIAL SUBTROPICAL HIGH MIGRATION

- Taylor, S. R., and S. M. McLennan (1985), *The Continental Crust: Its Composition and Evolution – an Evaluation of the Geochemical Record Preserved in Sedimentary Rocks*. 312 pp., Blackwell Sci., Oxford, U. K.
- Tchakerian, V. P., and N. Lancaster (2002), Late Quaternary arid/humid cycles in the Mojave Desert and western Great Basin of North America, *Quat. Sci. Rev.*, *21*, 799–810.
- Tertian, R., and C. Claisse (1982), *Principles of Quantitative X-ray Fluorescence*, 320 pp., Heydon, London.
- Thunell, R. C. (1998), Seasonal and annual variability in particle fluxes in the Gulf of California, a response to climate forcing, *Deep Sea Res., Part I*, *45*, 2059–2083.
- Thunell, R. C., C. J. Pride, E. G. Tappa, and F. E. Muller-Karga (1993), Varve formation in the Gulf of California, insights from times series sediment trap sampling and remote sensing, *Quat. Sci. Rev.*, *12*, 451–464.
- Thunell, R. C., C. J. Pride, and E. Tappa (1994), Biogenic fluxes and accumulation rates in the Gulf of California, *Geology*, *22*, 303–306.
- Thunell, R. C., E. Tappa, and D. M. Anderson (1995), Sediment fluxes and varve formation in Santa Barbara Basin, offshore California, *Geology*, *23*, 1083–1086.
- Thunell, R., C. Pride, P. Ziveri, F. Muller-Karger, C. Sancetta, and D. Murray (1996), Plankton response to physical forcing in the Gulf of California, *J. Plankton Res.*, *18*, 2017–2026.
- Yamamoto, M., M. Yamamuro, and Y. Tanaka (2007), The California Current system during the last 136,000 years, response of the North Pacific High to precessional forcing, *Quat. Sci. Rev.*, *26*, 405–414.
- Ziveri, P., and R. C. Thunell (2000), Coccolithophore export production in Guaymas Basin, Gulf of California, response to climate forcing, *Deep Sea Res., Part II*, *47*, 2073–2100.